# Climate Data Record (CDR) Program

## Climate Algorithm Theoretical Basis Document (C-ATBD)

## Special Sensor Microwave/Imager (SSM/I)

## V2 Brightness Temperature – CSU

## Special Sensor Microwave/Imager (SSM/)

## V2 Brightness Temperature – CSU Gridded

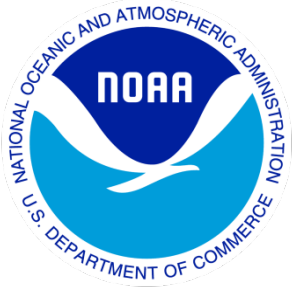



| | |
|---|---|
| CDR Program Document Number: | CDRP-ATBD-0337 |
| Configuration Item Number: | 01B-15 and 01B-15a |
| Dataset Version/Revision: | V02R00 |
| Document Revision 3: | June 16, 2021 |

# REVISION HISTORY

| Rev. | Author | DSR No. | Description | Date |
|---|---|---|---|---|
| 1 | Wesley Berg, Colorado State University | DSR-394 | Initial Submission to CDR Program | 07/11/2013 |
| 2 | Wesley Berg, Colorado State University | DSR-923 | Addition of daily gridded FCDR and ICDR brightness temperature data files | 04/15/2015 |
| 3 | Wesley Berg, Colorado State University | DSR-1580 | Updated for FCDR Version 2 release (V02R00) | 6/16/2021 |
| | | | | |
| | | | | |
| | | | | |
| | | | | |
| | | | | |
| | | | | |
| | | | | |

# TABLE of CONTENTS

# LIST of FIGURES



# LIST of TABLES

# 1. Introduction

## 1.1 Purpose

The purpose of this document is to describe the algorithm used to create the Colorado State University (CSU) Fundamental Climate Data Record (FCDR) of brightness temperature data from the series of six Special Sensor Microwave/Imager (SSM/I) instruments on board the Defense Meteorological Satellite Program (DMSP) spacecraft F08, F10, F11, F13, F14 and F15. The actual algorithm is defined by the computer program (code) that accompanies this document, and thus the intent here is to provide a guide to understanding that algorithm, from both a scientific perspective and to assist a software engineer performing an evaluation of the code.

## 1.2 Definitions

None currently.

## 1.3 Referencing this Document

This document should be referenced as follows:

SSM/I Brightness Temperature – CSU and SSM/I Brightness Temperature – CSU Gridded - Climate Algorithm Theoretical Basis Document, NOAA Climate Data Record Program CDRP-ATBD-0337 Rev. 3 (2021). Available at http://www.ncdc.noaa.gov/cdr/operationalcdrs.html

## 1.4 Document Maintenance

Synchronization between this document and the algorithm is achieved through version and revision numbers. The dataset version and revision numbers found on the front cover of this document can be compared with the values of `VERSION` and `REVISION` in the source file `params.h`. If the document applies to the algorithm, then these numbers will match. If they don't match and it is found that the document needs to be updated, then the header comment in the file `ssmi_fcdr.c` should be consulted – under its `HISTORY` section is a description of the changes for each version and revision from which the necessary updates to this document can be made.

# 2. Observing Systems Overview

## 2.1 Products Generated

The data product generated by this algorithm is the Fundamental Climate Data Record (FCDR) of brightness temperature (Tb) data from the SSM/I sensors, including five low-resolution channels (Tb19v, Tb19h, Tb22v, Tb37v, Tb37h) and two high-resolution channels (Tb85v, Tb85h), stored in netCDF version 4.0 files that include the necessary metadata and supplementary data fields. Additionally, a daily gridded version of the FCDR Tb data is produced on a 0.25 x 0.25 degree equal angle global grid. The data fields for both the pixel resolution and gridded FCDR data files are described in detail section 3.4.7 below.

## 2.2 Instrument Characteristics

Data supplied to this algorithm was collected by SSM/I instruments on board the DMSP satellites F08, F10, F11, F13, F14 and F15. The DMSP series satellites are in sun-synchronous polar orbits at an altitude of approximately 830 km. The instrument is a seven channel linearly polarized passive microwave radiometer operating at frequencies of 19.35, 22.235, 37.0 (low-resolution), and 85.5 (high-resolution) GHz. The 19.35, 37.0, and 85.5 GHz frequencies have dual-polarization (vertical and horizontal), and the 22.235 GHz frequency has only vertical polarization. The instrument scans through 102 degrees for each scanning revolution producing a swath approximately 1400 km wide. The A-scan data is recorded for all channels, while the B-scan data is only recorded for the high-resolution channels. This configuration is shown in Figure 1. Detailed specifications for the spacecraft and instrument are given by Hollinger et al. (1987) and Hollinger (1989, 1991).

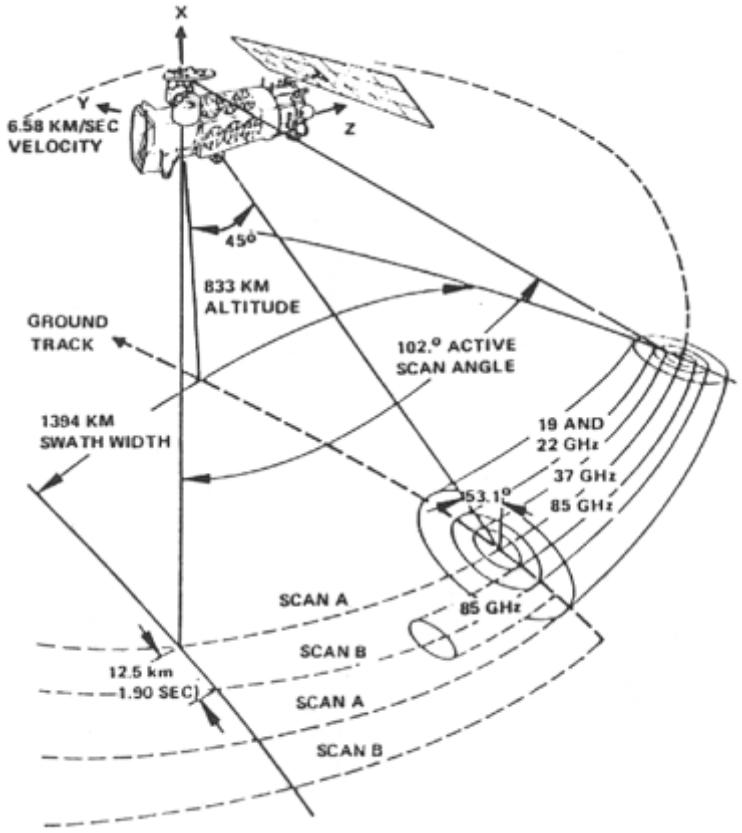


Figure 1: SSM/I Scan Configuration.

## SSM/I channel characteristics:

| **Center Frequencies (GHz)** | **19.35** | **19.35** | **22.235** | **37.0** | **37.0** | **85.5** | **85.5** |
|---|---|---|---|---|---|---|---|
| Polarization | V | H | V | V | H | V | H |
| Bandwidth (MHz) | 250 | 250 | 250 | 1000 | 1000 | 1500 | 1500 |
| Sensitivity (K) | 0.6 | 0.6 | 0.6 | 0.6 | 0.6 | 1.1 | 1.1 |
| EFOV<br>(km along track x km across track) | 69 x 43 | 69 x 43 | 50 x 40 | 37 x 28 | 37 x 29 | 15 x 13 | 15 x 13 |
| Sampling Interval<br>(km along track x km across track) | 25 x 25 | 25 x 25 | 25 x 25 | 25 x 25 | 25 x 25 | 12.5 x 12.5 | 12.5 x 12.5 |
| Integration Time (msec) | 7.95 | 7.95 | 7.95 | 7.95 | 7.95 | 3.89 | 3.89 |
| Main Beam Efficiency (%) | 96.1 | 96.5 | 95.5 | 91.4 | 94.0 | 93.2 | 91.1 |
| Beamwidth (half-power, degrees) | 1.87 | 1.87 | 1.65 | 1.10 | 1.10 | 0.43 | 0.45 |

Table 1: SSM/I channel characteristics

Channel characteristics shown in Table 1 are from:

- Hollinger et al. (1987), Table 2.1 (EFOV, Beamwidth), Section 2.2 (Sampling Interval), and Table 2.2 (Beam Efficiency).
- Raytheon (2000), Table 3-1 (Integration Time).

# 3. Algorithm Description

## 3.1 Algorithm Overview

The algorithm operates on input BASE files, which contain the original antenna temperature (Ta) and calibration data for seven channels as input, processes the data through several stages, and creates output FCDR files of brightness temperature (Tb) for all seven channels. The processing stages include: calculate spacecraft ephemeris; calculate pixel geolocation; quality control; cross-track bias correction; convert antenna temperatures to brightness temperatures via an antenna pattern correction; intercalibrate to get physically a consistent Tb record across the different satellites; and correct the Tb22v channel of F15 after RADCAL activation in August of 2006 for Tb contamination.

## 3.2 Processing Outline

The steps of this algorithm include reading the input data, seven sequential processing stages each of which can be turned on or off with a flag in the code, and writing the output data file. Each stage is described in this section. The processing flow is shown in Figure 2.

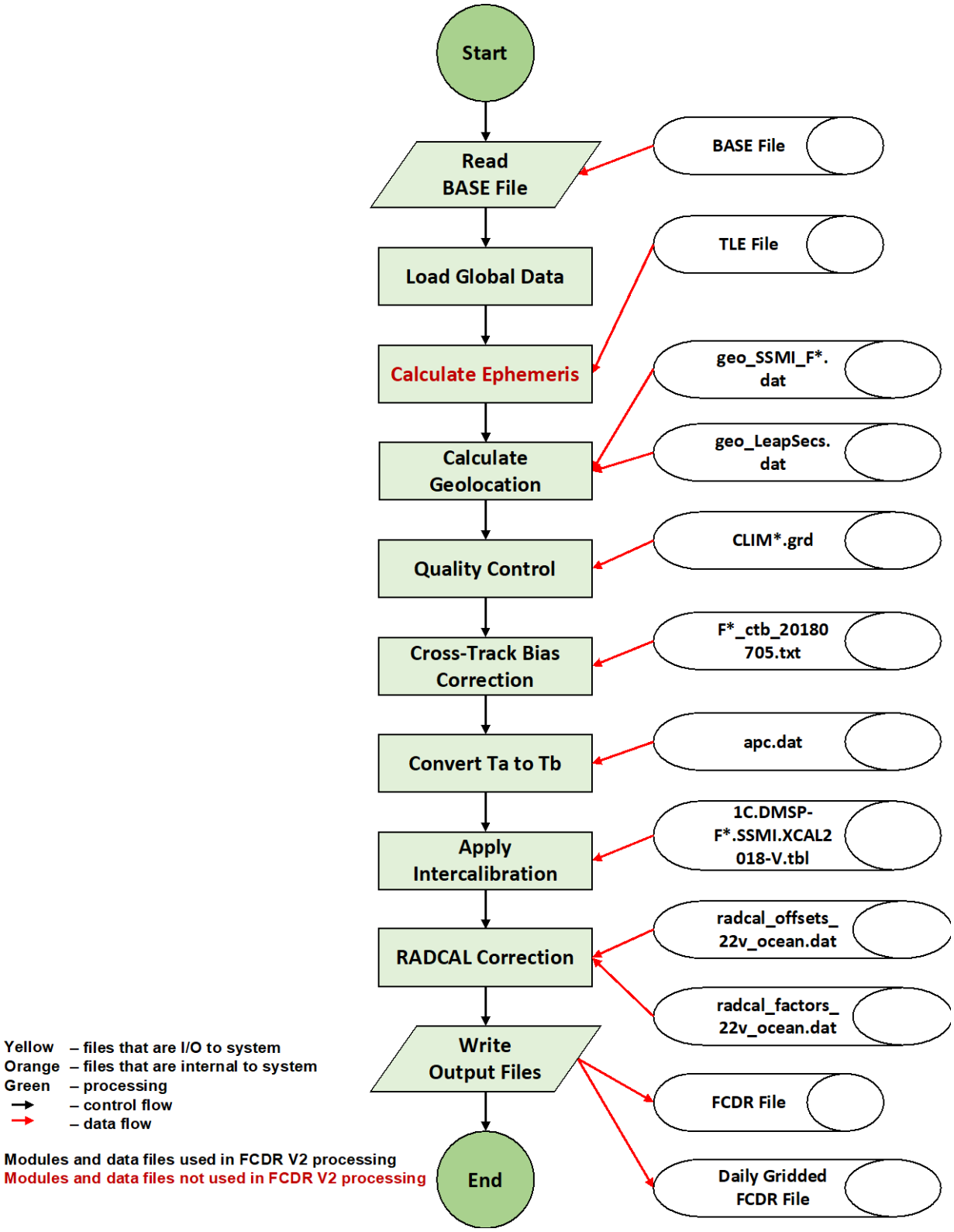


Figure 2: Flowchart for SSM/I version 2 processing

### 3.2.1 Read Input

Data from the input BASE file (see section 3.3.3), optional two-line element (TLE) files (see section 3.3.2), and look-up tables (see section 3.4.5), is read and stored in global variables that are accessed by the subsequent steps. Space is allocated to store output data and certain fields are prepopulated from the input data.

### 3.2.2 Calculate Ephemeris

The spacecraft position and velocity have been precomputed from TLE orbital elements files and are stored in the input BASE files. Because the TLE files are not generally publicly available and cannot be publicly distributed at this time, the algorithm currently uses the precomputed spacecraft position and velocity data stored in the input BASE files. The Simplified General Perturbations (SGP4) code used to compute the spacecraft position and velocity from the TLE files, however, is included as part of the FCDR algorithm package. Given available TLE files the option to recompute the spacecraft ephemeris is available within the code. For the FCDR processing this option was turned off and the position and velocity information stored in the BASE files was used. When this processing stage is turned on, a flag additionally allows a choice between recomputing the ephemeris from the TLE when the time of the TLE is closer than that used in the BASE file or regardless of timing.

### 3.2.3 Calculate Geolocation

Taking as input the spacecraft position and velocity along with data on the sensor mount angles and spacecraft orientation data, the geolocation or latitude and longitude of each pixel is calculated and stored. Additional information related to the spacecraft view angles and associated sun angles are also computed. These include the satellite zenith and azimuth angles and solar zenith and azimuth angles, which provide the direction of the satellite and the sun from the normal to the Earth for each pixel. The satellite zenith angle is also referred to as the Earth incidence angle (EIA), which is important for retrieval algorithms as it impacts the resulting Tb. The sun glint angle is also computed and provided to identify potential specular reflection from the sun over water surfaces that may also impact retrieval algorithms. Additional information computed at this stage includes angles relating the position of the sun relative to the spacecraft direction of motion, whether the spacecraft is in the Earth's shadow, and the time since the spacecraft entered into the Earth's shadow or time since eclipse. Only the EIA and sun glint angles are written out in the FCDR files, but the other angles/fields are computed for analysis purposes. Offsets to the spacecraft/sensor roll and pitch were estimated based on an analysis of simulated minus observed cross-track bias patterns. Offsets in the roll direction result in a slope across the scan, while offsets in the pitch direction result in an arc shaped pattern in the cross-track biases. A coastline analysis, described in detail by Berg et al. (2018), was used to solve for offsets in the spacecraft/sensor yaw direction along with delta EIA offsets and timing offsets.

### 3.2.3.1 Pixel Geolocation (Geodetic Latitude and Longitude)

The process for calculating the pixel latitude and longitude starts with the calculation of the Instantaneous Field-Of-View (IFOV) matrix in sensor coordinates. Several rotations are required to obtain the IFOV in Geocentric Inertial (GCI) coordinates. First there is the sensor-to-spacecraft rotation that obtains the IFOV relative to the spacecraft. Next there is the spacecraft-to-orbital (geodetic nadir pointing) rotation that obtains the IFOV relative to the path of the spacecraft. Finally, there is the orbital-to-GCI rotation that obtains the IFOV in GCI coordinates. With the IFOV in GCI coordinates, the intersection of the IFOV with the oblate spheroid used to model Earth is calculated and this is then used to get geocentric, then geodetic latitude and longitude.

### 3.2.3.2 Satellite Zenith and Azimuth

In order to calculate the satellite zenith (i.e. Earth Incidence Angle or EIA) and azimuth angles, it is necessary to first determine the local zenith (up), north and east vectors. The satellite zenith angle is the angle between the local up vector and the pointing vector and the azimuth angle is the angle between the projection of the pointing vector on the surface and the local north vector where positive azimuth angle is clockwise when viewed from above.

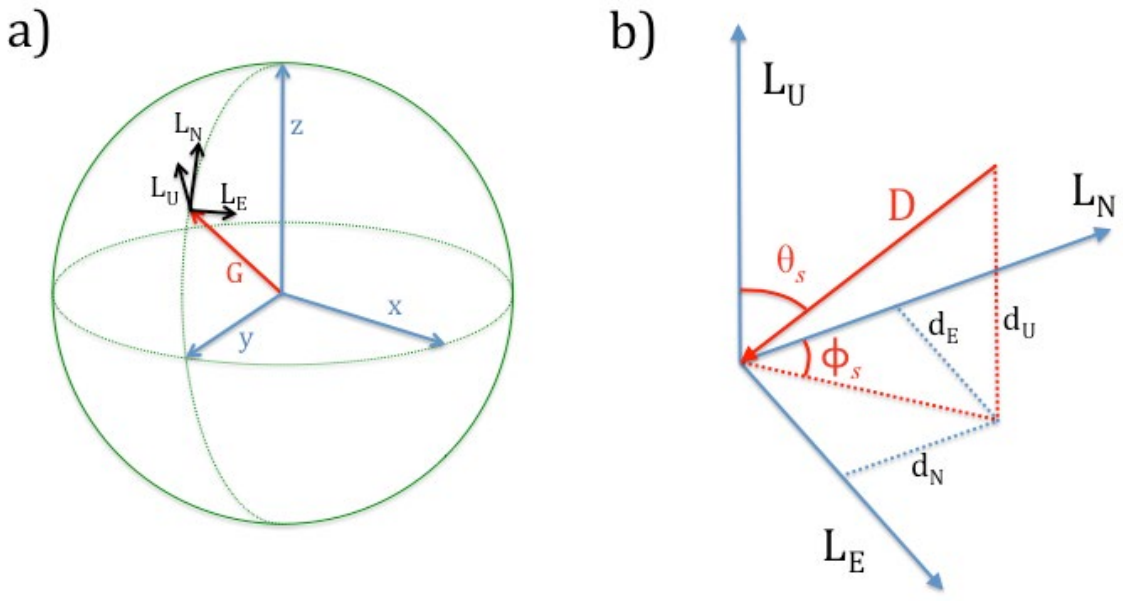


Figure 3: Diagram showing (a) the local zenith (up), east and west vectors on Earth's surface relative to the GCI frame; and (b) the zenith and azimuth angles relative to the pointing vector **D**.

### 3.2.3.3 Solar Angles

Various solar angles are calculated based on the Sun position vector in GCI coordinates determined as described in Appendix C, section C4 of Sapiano et al. (2010). Solar beta

angle, sun glint angle, and solar zenith and azimuth angles are found using the Sun position vector. The time since eclipse is also calculated to provide information on solar heating of the spacecraft based on how long it has been in sunlight or shadow.

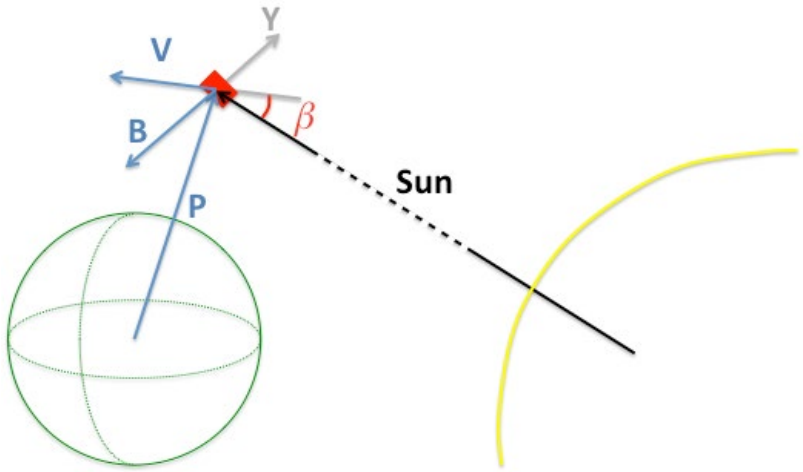


Figure 4: Diagram of angles associated with the solar beta angle.

### 3.2.4 Quality Control

The quality control processing stage (*qual_control.c*) consists of multiple procedures, which check for potentially erroneous data, correct it if possible, and set the corresponding quality flag. Note that the quality control is done on the input Ta prior to the application of the antenna pattern correction (APC). The quality flag values are specified in the file metadata and are defined in the include file *quality_flags.h*. There is a quality flag value for each scan and pixel, with one flag for the low-resolution channels, and one for the high-resolution channels. The flag values consist of three categories with a value of zero indicating good data, values between 1 and 99 indicating a warning or caution, and values from 100 and above indicating an error. For pixels with flag values >= 100 the affected Tb are subsequently set to missing. The warning flags provide the user information on potential issues, which are often algorithm dependent. For example, a quality flag value of 1 indicates possible sun glint, which is only an issue over reflective surfaces like water and is not an issue at all for some retrievals. A short description of the various quality control procedures follows.

#### 3.2.4.1 Correct Ta

Erroneous spikes in hot and cold loads are identified. For affected data, count values are reconstructed from antenna temperatures, the hot and cold load values are interpolated from neighboring scans, corrected antenna temperatures are then computed, and the quality flag is set to indicate that this Ta correction has been applied. This correction is described in detail in Berg and Rodriguez-Alvarez (2012).

#### 3.2.4.2 Check BASE file

Quality control checks done during the creation of the BASE files include checks for erroneous pixel geolocation due to time offset errors. This routine sets the associated FCDR quality flag and sets the affected output Tb to missing.

#### 3.2.4.3 Check Geolocation

For data where the original pixel location, given by latitude and longitude, is more than 100 kilometers away from the computed location, the Ta data are set to missing and a quality flag set to indicate a geolocation issue.

#### 3.2.4.4 Check Sensor

Data is set to missing and the quality flag is set for known sensor issues as determined from documented issues and data monitoring. For example, dates corresponding to the failure of first the 85v and then the 85h channels on the F08 SSM/I were determined from an analysis of the data and hardcoded into this routine. The details of which satellites and orbits/dates have known sensor issues are coded into the function that performs this check rather than read from a file.

#### 3.2.4.5 Check Climatology

For each channel, scans where a significant fraction of pixels differ from the climatological mean values (determined as described in section 3.4.5.2) by more than 3 standard deviations are flagged. Two levels of climatology checks are identified. A climatology warning flag is set for scans near the threshold (within 5%) and the Ta data are retained. For scans exceeding this threshold, an error flag value is set in the corresponding quality flag and the Ta data is set to missing.

#### 3.2.4.6 Check Pixel

Pixels where the distance between adjacent pixels along a scan is outside minimum and maximum thresholds, the Ta values are outside minimum and maximum thresholds (i.e. nonphysical), or the pixel latitude/longitude is out of range, have the appropriate quality flag set and the affected Ta are set to missing.

### 3.2.5 Cross-track Bias Correction

A falloff in the Tb occurs near the edge of the scan due to obstructions affecting the side lobes of the antenna pattern. The most pronounced decrease is on the right side of the scan, which results in a decrease in the mean observed Tb of several percent or more relative to the center of the scan. As described above in the geolocation description, roll and pitch offsets were first computed from simulated minus observed Tb values as a function of pixel position across the scan. The roll and pitch offsets were computed based on simulated slope and arc patterns across the center of the scan. The roll and pitch offsets were then added into the geolocation calculation to effectively remove

these patterns and the results were subsequently verified to ensure the absence of any residual changes across the center portion of the scan.

To account for the falloff at the edge of the scan, an analysis over both clear-sky ocean (i.e. cold scenes) and vegetated land (i.e. warm scenes) was done for each sensor. Based on this analysis an offset and temperature-dependent scale factor was computed for each pixel position relative to the center of the scan. The resulting scale and offset values for each sensor and channel are stored in the files F*_ctb_20180705.txt. The cross-track biases are subsequently removed from the Tb to ensure consistent values across the entire scan for each channel regardless of the scene temperature. These correction coefficients are obtained from the look-up table described in section 3.4.5.3.

### 3.2.6 Ta to Tb Conversion

Based on a pre-launch analysis of the antenna pattern, described by Colton and Poe (1999), an antenna pattern correction (APC) is applied to the observed Ta to calculate the physical Tb. The Tb is calculated using equation 1, which involves four coefficients for each sensor/channel. This attempts to correct for spillover losses, cross-polarization coupling between channels, and sidelobe contamination. The coefficient $C_1$ is multiplied by the cross-polarized pixel whereas the coefficient $C_2$ is multiplied by the previous adjacent pixel Ta and the coefficient $C_3$ by the next adjacent pixel Ta. The coefficient values are stored in the look-up table described in section 3.4.5.4.

$$Tb_{v,h} = C_0 * Ta_{v,h}(n) + C_1 * Ta_{h,v}(n) + C_2 * Ta_{v,h}(n-1) + C_3 * Ta_{v,h}(n+1) \qquad (1)$$

To calculate Tb22v, the above equation requires a Ta22h value, which following Colton and Poe (1999), is obtained by the following:

$$Ta_{22H} = 0.653\, Ta_{19H} + 96.6 \qquad (2)$$

While the APC coefficients for each of the six SSM/I sensors are provided by Colton and Poe (1999), the decision was made by FNMOC to use the F13 values for F14 and F15 as well for the operational processing of the sensor data record (SDR) files. This was confirmed to be the case by comparing the computed Tb with the SDR Tb values. While detailed information regarding this decision by FNMOC was not available, we chose to be consistent with the SDR record and to account for any residual differences in our subsequent intercalibration analysis.

### 3.2.7 Intercalibration

One of the most significant changes to the calibration for Version 2 of the FCDR data is the use of the Global Precipitation Measurement (GPM) Microwave Imager (GMI) as the calibration reference. Pre- and post-launch characterization of the GMI calibration have shown it to be extremely well calibrated and stable [Berg et al., 2016; Wentz and Draper, 2016]. Previously F13 was chosen as a calibration reference due to its longevity and stable orbit, however, it was recognized that F13 does not represent a high-quality

calibration reference in an absolute calibration sense. The intercalibration of the SSM/I sensors relative to GMI is also a two-point adjustment based on comparisons over clear-sky oceans (cold scenes) and vegetated land surfaces (warm scenes), whereas the V1 calibration was a single offset value irrespective of the scene temperature. Details and results of the intercalibration are provided in Berg et al. 2018.

It is important to note that intercalibration does not imply that the resulting Tb will be identical between sensors. Instead, the purpose of the intercalibration is to ensure that measurements between the sensors are "physically" consistent. Physical differences between sensors including diurnal sampling differences and view angle or EIA differences remain and must be accounted for by the geophysical retrieval algorithms.

### 3.2.8 RADCAL Correction

The activation of RADCAL on F15 in August 2006 caused significant contamination of the TB22V channel. This contamination is removed using an approach similar to that of Remote Sensing Systems described in Hilburn (2009) and Hilburn and Wentz (2008). Our resulting correction is given by the equation

$$Tb22v_{corr} = Tb22v - offset(scan\ position) * factor(hotload) \qquad (3)$$

where $Tb22v_{corr}$ is the corrected Tb, $offset(scan\ position)$ and $factor(hotload)$ are obtained from the look-up tables described in section 3.4.5.6. The values stored in these look-up tables were derived by first using a linear regression model to predict Tb22v from the other 6 channels using 2005 data (before RADCAL activation) using non-precipitating ocean scenes (based on the filter developed by Stogryn et al., 1994). The resulting prediction is:

$$Tb22v_{pred} = 0.1444\ Tb19v + 1.1013\ Tb19h + 0.6625\ Tb37v - 1.0975\ Tb37h +$$

$$0.0062\ Tb85v + 0.3245\ Tb85h + 3.5265 \qquad (4)$$

This prediction was found to match the observed data reasonably well. It was then used to predict Tb22v for 2007 data (after RADCAL activation). For each scan position, the mean difference $Tb22v - Tb22v_{pred}$ for 2007 ocean data is the value stored in the look-up table as $offset(scan\ position)$. Simply subtracting this offset from Tb22v results is a reasonable correction for much of the RADCAL-contaminated data, but where the hotload is colder than normal it results in large spikes that indicate a problem with this correction attempt. This is addressed by instead using the multiplicative model defined by 3 as the correction. For 2007 through 2011 data, the values $(Tb22v - Tb22v_{pred}) / offset(scan\ position)$ were calculated, then binned as a function of hotload using 1 Kelvin bins. The mean value of each bin is stored in the look-up table as $factor(hotload)$. A time series of the observed and corrected Tb22v data is shown in Figure 5.

The estimated error in $Tb22v_{corr}$ depends on the hot load temperature, varying from around 3.5 K for values above 290 K to over 5 K when the hot load falls below 270 K.

These error estimates show that RADCAL-corrected data is not suitable for climate applications. Hilburn and Wentz (2008) came to the same conclusion that the RADCAL-corrected data may be suitable for many weather applications, but is not of suitable accuracy/stability and therefore should not be used in climate analyses. The quality flag for the low-resolution channels of the RADCAL-corrected Tb22v data (F15 only after August 13, 2006) is set to a value of 13 to indicate that it is unsuitable for climate applications.

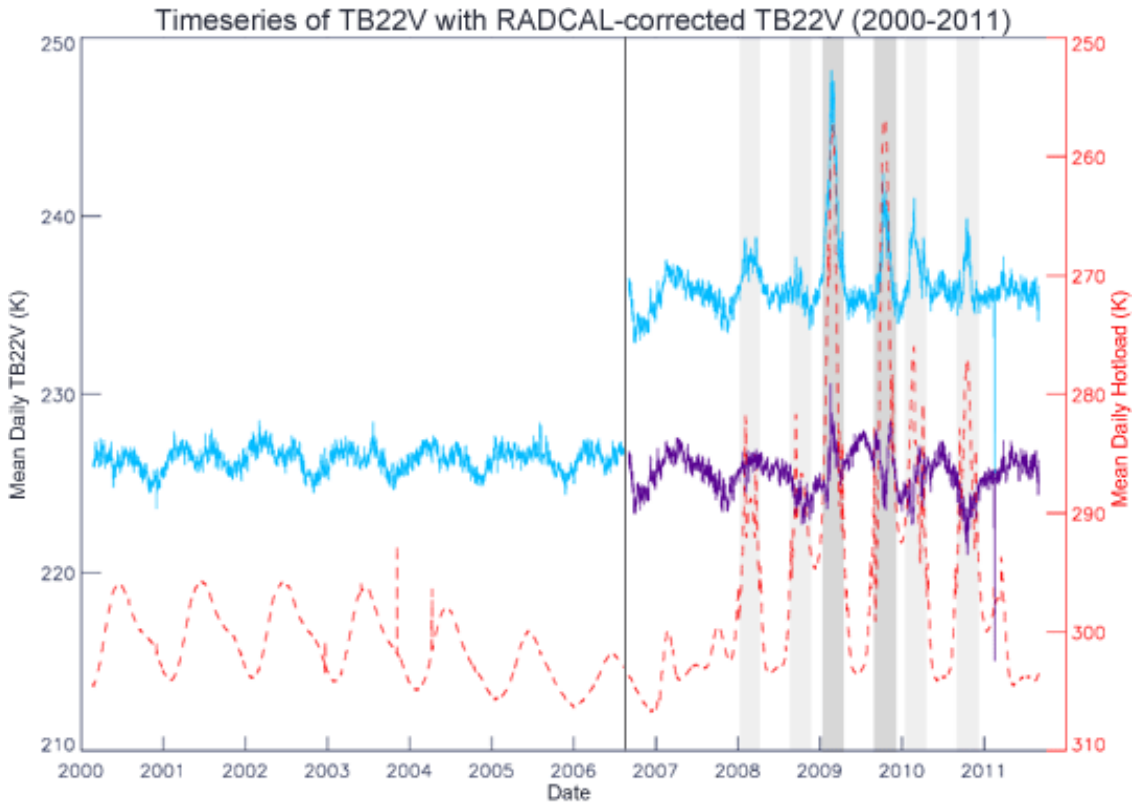


Figure 5: Timeseries of original observed Tb22v (blue) and the RADCAL-corrected Tb22v (purple) based on Equation 3 for ocean scenes between 80S and 80N. The corresponding hot load temperature (dashed red line) is also shown with moderate dips in the hot load temp indicated by the light gray shaded regions and large dips indicated by the dark gray shaded regions. The black vertical line in August of 2006 indicates when the RADCAL beacons were activated.

### 3.2.9 Write Output

The output FCDR files and daily gridded FCDR files (described in section 3.4.7) containing the final Tb values with corrections and intercalibration applied are written out in NetCDF4. Note that there is an option in the software to write out an XBASE file, which contains all of the data fields in the input BASE file along with the output FCDR variables and the various satellite/sun angles which are computed but not output in the

FCDR file. This option is provided for users wanting to further information to investigate calibration issues etc.

# 3.3 Algorithm Input

## 3.3.1 Primary Sensor Data

The raw sensor data are sensor counts from SSM/I instruments. The sensor counts are converted to antenna temperature (Ta) by applying the calibration from the cold sky and calibration target views each scan and stored in the Temperature Data Record (TDR) files created by the Shared Processing Network Data Exchange Format (SPN DEF). These TDR files are subsequently converted into BASE files, which are used as input for the algorithm and are described in section 3.3.3 below.

## 3.3.2 Ancillary Data (optional)

The Two-Line Element (TLE) data created by NORAD containing the satellite orbital elements are used to determine the satellite's position and velocity. The TLE files are in the NORAD TLE format consisting of a title line, which is the satellite name, followed by two lines of formatted text. By default, the algorithm uses the precomputed spacecraft position and velocity information stored in the input BASE files.

## 3.3.3 Derived Data

The input data files used for the FCDR processing are referred to as BASE files. These files contain all of the information from the original source TDR files with the following changes/additions. The BASE files have been reorbitized into single orbit granules with duplicate scans removed and spacecraft position and velocity based on the TLE data added (for later use to calculate geolocation). The BASE files are written in NetCDF4 format with metadata added. Except for duplicate scans, none of data from the original TDR files is changed or removed. The concept of the BASE files is to preserve the original data in an easy-to-read self-describing format and to simplify the FCDR processing. The format specification for the BASE files is described in detail in the *SSM/I BASE file Format Specification* available at (http://rain.atmos.colostate.edu/FCDR/Archive_Docs/formatspecs/ssmi_base_format_spec_v1.pdf).

## 3.3.4 Forward Models

No forward models are used in the FCDR processing, however, the development of the intercalibration offsets required radiative transfer calculations to account for differences in EIA between sensors. The models used include MonoRTM version 5.3 developed by AER (Clough et al. 2005) for the atmospheric absorption model and the model by Meisner and Wentz (2012) for ocean emissivities. These models are only used to derive the roll and pitch offsets, the coefficients used in the intercalibration and some of the other corrections.

# 3.4 Theoretical Description

The software developed for the SSM/I FCDR processing is a stepwise approach described in Section 3.2. This involves reading the input BASE file along with the necessary data coefficient files etc., quality control procedures, calculation of the spacecraft position and velocity (optional) and pixel geolocation, application of cross-track bias corrections, APC correction to compute Tb from Ta, application of intercalibration offsets, and correction for RADCAL interference in the F15 22 GHz channel after August of 2006.

## 3.4.1 Physical and Mathematical Description

### 3.4.1.1 Physical Background

Passive microwave sensors, such as the SSM/I, measure the microwave radiation emitted by Earth's surface and atmosphere and interacting with the atmosphere through absorption, scattering, and transmission before reaching the sensor. The amount of absorption and scattering of radiation as it travels through the atmosphere depends on the wavelength (or equivalently, frequency) of the radiation and on the state of the atmosphere (e.g. amount of water vapor, rain, cloud, etc.).

The emission of radiation from Earth's surface and atmosphere is described by Planck's law with the deviation of real materials from ideal blackbodies accounted for by the emissivity (ε) of the material. Directly above the surface the brightness temperature (Tb) of a scene at a given frequency is the product of the emissivity of the surface and the scene temperature:

$$Tb = \varepsilon \, T_{actual} \qquad (5)$$

The radiation emitted from the surface is subsequently modified by the atmosphere before reaching the satellite sensor, which provides information on the state of the atmosphere. Information about the amount of water vapor, liquid water and ice is inferred from SSM/I data by exploiting known changes in the thermal spectrum due to the absorption, emission, and scattering of radiation. The SSM/I User's Interpretation Guide (Raytheon 2000), section 2, provides theory of remotely sensed electromagnetic radiation – especially microwave radiation – and how it is used to retrieve geophysical atmospheric and surface parameters.

### 3.4.1.2 Astronomical and Geographical Calculations

The Simplified General Perturbations (SGP4) orbital model (Vallado et al., 2006) is used to calculate perturbations of the satellite orbit due to effects of the sun, moon, Earth's oblateness, etc. The orbital position and velocity of the spacecraft calculated using this model are used along with other satellite and sensor parameters (as described in

sections 3.2.3 and 3.4.5.1) to compute the corresponding geolocation or latitude and longitude of each individual pixel or Earth scene.

#### 3.4.1.3 Sensor Characteristics

The physical sensor characteristics and configuration are described in Section 2.2.

#### 3.4.1.4 Simplifications and Approximations

In the quality control processing stage (see section 3.2.4.3), the distance between pixel locations is approximated by using a sphere to model the Earth.

### 3.4.2 Data Merging Strategy

The original sampling provided by the six SSM/I sensors is preserved in the output FCDR data with no merging of the resulting data in either space or time. The resulting FCDR Tb from each of the six sensors are intercalibrated to be physically consistent with the observed Tb from the calibration reference sensor (i.e. GPM GMI). Differences between the various sensor Tb due to the local observing time or variations in the view angle/EIA remain. Accounting for these differences and merging the data from the various sensors is left to TCDR developers.

### 3.4.3 Numerical Strategy

The subroutines to compute the spacecraft position and velocity from the TLE files were implemented based on the North American Aerospace Defense Command (NORAD) SDGP4 code (Vallado et al., 2006). Additional details are provided in the header of the subroutine *sdgp4.c.* Details on the numerical calculations of the pixel geolocation and associated angles are provided in CSU technical report by Sapiano et al. (2012).

### 3.4.4 Calculations

Details on the processing steps involved in the algorithm are provided in Section 3.2

### 3.4.5 Look-Up Table Description

Six stages of the algorithm use data that has been calculated and is stored in static look-up tables. The look-up tables used in each stage are described in this section.

#### 3.4.5.1 Calculate Geolocation

The geolocation calculation makes use of the look-up tables contained in the two text files listed below where F** is the satellite designation F08 through F15:

1. `geo_SSMI_F**.dat` – This file contains data lines which are pairs of a variable name and its value for a variety of time, geometry, sensor alignment, and spacecraft attitude variables.

2. `geo_LeapSecs.dat` – This file contains a line for each leap second adjustment since 1972 giving values for the Julian day, number of seconds, and sign of adjustment. This data is needed to convert between International Atomic Time (TAI) seconds and Universal Time (UT) seconds.

The geolocation code requires values for satellite and sensor parameters (satellite attitude, sensor alignment, sensor elevation offset and scan angle offset) which are stored in the files `geo_SSMI_F**.dat`. Published values for the sensor delta elevation angles based on pre-launch measurements are used (Table VI in Colton and Poe, 1999). For scan angle offset, sensor alignment, and satellite attitude, values are determined from the data by the method described in Berg et al. (2018) to correctly locate the boresight.

#### 3.4.5.2 Climatological Quality Check

The mean and standard deviation of the antenna temperatures for each latitude/longitude grid position, each channel, and each month are stored in binary data files named `CLIM01.grd` for January up to `CLIM12.grd` for December. The climatological quality check subroutine flags where the fraction of pixels in a scan differing from the mean by more than 3 standard deviations exceeds a threshold.

#### 3.4.5.3 Cross-track Bias Correction

The cross-track bias correction coefficients for each satellite are stored in the binary files `F**_cbt_`*`yyyymmdd`*`.txt` where F** is the satellite name F08 through F15 and yyyy*mmdd* is the date that the file was created (i.e. 20180705). These files contain the correction coefficients including a scale and offset value for each scan position for each channel.

#### 3.4.5.4 Ta to Tb Conversion

The antenna pattern correction (APC) coefficients used to convert Ta to Tb are stored in the text file `apc.dat`. The derivation of these coefficients is described in Colton and Poe (1999). The coefficients were obtained from Fleet Numerical Meteorology and Oceanography Center (FNMOC) and are from the operational processing code. The APC coefficients obtained from FNMOC are similar to those found in Colton and Poe (1999), Table II (p. 421), columns C0, C1, C2 and C3, but have the following differences:

- The values for satellite F08 channel 85H are different.
- For all satellites and channels, the values of C1, C2 and C3 are negated.
- For satellites F14 and F15, we use the F13 coefficients to be consistent with how the SDR is produced (as explained in an email from Gene Poe with the NRL dated Dec 10, 2004).

#### 3.4.5.5 Intercalibration

The calibration offsets used for intercalibration between the different satellites are stored in the text file `1C.DMSP-F??.SSMI.XCAL2018-V.tbl`. These are the same intercalibration files developed and applied for V07 of the NASA Level 1C intercalibrated Tb dataset. As described above, a two-point calibration adjustment is performed for each channel based on cold and warm scene differences with GMI.

#### 3.4.5.6 RADCAL Correction

The Tb22v channel of F15 for times after RADCAL activation is corrected using the Tb22vcorr = *Tb22v – offset(scan position) * factor(hotload)* *(* in section 3.2.8 and the quality flag set to indicate that the corrected data is unsuitable for climate applications. This calculation uses two look-up tables stored in the following text files:

1. `radcal_offsets_22v_ocean.dat` – The offset for each low-resolution scan position 1 to 64.

2. `radcal_factors_22v_ocean.dat` – The factors for each 1 Kelvin hot load temperature bin.

### 3.4.6 Parameterization

The antenna pattern correction or APC is a parameterization of the measured antenna pattern. It is described above in section 3.2.6 and by Colton and Poe (1999).

### 3.4.7 Algorithm Output

For each input BASE file, the algorithm produces an output FCDR file in NetCDF4 format. There are approximately 15 files per sensor per day and each file is approximately 5.8 Mbytes. Empty files containing only global metadata fields are produced for orbits with no available input TDR data. The FCDR file contains the final intercalibrated Tb for each channel along with pixel latitude and longitude, time for each scan, spacecraft position, quality flags, sun-glint angle, and fractional orbit number with the necessary metadata and supplementary data fields. Two sets of variables are provided. One set corresponds to the five low-resolution channels and the other to the two high-resolution (85 GHz) channels. The data are truncated to the nearest 0.001 degree for the lat/lon values and to the nearest 0.01 K for the Tb and view angles. Internal NetCDF data compression is used to compress the files.

Daily gridded FCDR files are also produced. These files contain Tb values gridded on a global equal angle grid at 0.25 x 0.25 degree resolution. Separate grids are produced for the ascending and descending scans. At higher latitudes where multiple swaths can overlap during the course of the day, the grid only contains values from the most recent (or latest) overpass values. In addition to the gridded Tb values for the seven SSM/I channels, the view angle or Earth Incidence Angle (EIA), time-of-day (hour, minute and

second), and number of pixels in the grid box are provided for each channel and grid point. Note that data are not interpolated at high latitudes to fill missing boxes within the scan, but are replicated from the nearby pixel values.

A detailed specification of the format of the FCDR files is provided in the *SSM/I FCDR File Format Specification*. (http://rain.atmos.colostate.edu/FCDR/Archive_Docs/formatspecs/ssmi_fcdr_format_spec_v1.pdf). Note that the format for the V1 and V2 FCDR files is identical.

# 4. Test Datasets and Outputs

## 4.1 Test Input Datasets

No test datasets were used to characterize the algorithm performance. Validation of the resulting FCDR data is described in Section 5.5.

## 4.2 Test Output Analysis

### 4.2.1 Reproducibility

As with the version 1 intercalibration (Sapiano et al. 2012, 2013), multiple intercalibration approaches were used to check for consistency and provide an estimate on the residual uncertainties (Berg et al. 2016; 2018).

### 4.2.2 Precision and Accuracy

The calibration accuracy of the SSM/I Tb is tied to that of the reference sensor (i.e. GPM GMI), which has been shown to be extremely well calibrated (Wentz and Draper, 2016). Uncertainties in the intercalibration estimates varies by channel and scene temperature, but they are generally within ~1.0 K for F11, F13, F14 and F15. For these

sensors, intercalibration comparisons were done based on double differences with TRMM TMI, which has been carefully intercalibrated to GPM GMI. This was done since all of the SSM/I sensors died prior to the launch of GPM, however, significant overlap is available between TRMM and F13, F14 and F15. The accuracy of the calibration decreases for the older SSM/I sensors since the results have to be daisy chained back in time. That is, F10 is calibrated to F11 and F08 is calibrated to F10. Analysis of F08 data is challenging since it was the only microwave imager in operation at the time and the 85 GHz channels failed relatively early on, but analysis of retrieved precipitation estimates indicates significantly larger calibration-related biases. Calibration precision of the SSM/I Tb is determined based on consistency between intercalibration approaches (Sapiano et al. 2013; Berg et al. 2016) and is generally within 0.5 K for most sensors/channels.

### 4.2.3 Error Budget

The intercalibration corrections applied in the processing stage described in section 3.2.7 were computed based on mean estimates from multiple techniques/results from the Precipitation Measurement Missions (PMM) XCAL intercalibration working group. Standard deviations of the individual double difference and/or other intercalibration estimates as well as between approaches provide a measure of the error in the intercalibration. Estimates of the residual intercalibration errors along with other error sources including sensor noise and the error in the GPM GMI calibration are given in Table 2.

| **Error Source** | **Error Magnitude** |
|---|---|
| Sensor Noise | 0.6 – 1.1 K |
| Intercalibration | 0.5 – 1.5 K (depending on sensor) |
| Absolute Calibration | 0.5 K |

Table 2: Error Budget

# 5. Practical Considerations

## 5.1 Numerical Computation Considerations

This algorithm doesn't use parallelization. No problems with matrix inversions are expected. Failure of the geolocation algorithm to produce a valid latitude and longitude can lead to missing pixel geolocation in rare instances. There are round-off errors in computations and conversions between different data types, which are expected and within the tolerance of the algorithm.

## 5.2 Programming and Procedural Considerations

The code implementing this algorithm uses standard procedural programming constructs such as: user-defined data structures to manage input and output data fields; control structures; functions; etc. No unusual programming techniques or optimizations are used as simplicity was an important design criterion. Specific features of the code include:

- A pattern used throughout much of the code is to loop through all the scans of an orbit granule and for each scan to loop through the low-resolution pixels and each low-resolution channel and the high-resolution pixels and each high-resolution channel.
- Each of the seven sequential processing stages of the algorithm can be turned on or off with a flag (these stages are described in section 3.2). This is useful for comparison and validation of individual processing stages, such as comparing the results of our Ta to Tb conversion (without intercalibration or any further corrections) with the SDR data set.

- Error and exception conditions are handled by direct checking of conditions/return codes in the main control flow, not by a language-supported exception construct.
- For efficiency (both execution speed and working storage space), extensive use is made of global variables.
- The source code is expected to build, and the resulting program to run, on a considerable range of different platforms. For more information on this, see section 5.6.

## 5.3 Quality Assessment and Diagnostics

See discussion on Section 5.5 on Validation. This includes application of geophysical retrievals and comparisons with other SSM/I FCDR datasets.

## 5.4 Exception Handling

Error and exception conditions are handled by direct checking of conditions/return codes in the main control flow rather than by a language-supported exception construct.

### 5.4.1 Conditions Checked

The following conditions identify errors that necessitate that the program terminate. They are trapped and the program prints a suitable message, then exits gracefully with a non-zero status indicating the type of error.

- If an incorrect number of arguments are supplied to the program, a usage message is printed and it exits with status 1.
- If there is an error opening or reading an input file, the program prints an error message and exits with status 2.
- If there is an error creating or writing to an output file, the program prints an error message and exits with status 2.
- If there are unrecoverable errors in the SGP4 orbital model code, an error message is printed and the program exits with status 5.

The following exceptions are trapped and recovered from by skipping over the item that can’t be processed, setting codes to track this, and continuing processing with the next item:

- In the geolocation code, where a vector is expected to intersect the oblate spheroid that models the Earth, the solutions of the equation are checked and if the expected intersection doesn’t exist, then the relevant data fields are set to missing and the geolocation is skipped over.

### 5.4.2 Conditions Not Checked

The following possible error condition is not checked for:

- In the unlikely event that the program would run out of memory, it would crash.

### 5.4.3 Conditions Not Considered Exceptions

Where data fields are missing or do not satisfy quality control checks (described in section 3.2.4), quality flags are set and for those quality issues classified as serious the corresponding data fields are set to indicate missing data. All corrections/conversions are applied only to non-missing data and if any processing stage identifies certain data as missing, it remains missing for all future processing stages. This is considered normal processing and not an exception condition.

## 5.5 Algorithm Validation

### 5.5.1 Validation during Development

Several methods were employed to validate the resulting FCDR data. These included the following.

1) Visual inspections and verification of the various corrections applied to the data. For example, as detailed by Berg et al. 2013 and Kroodsma et al. 2021, to verify the final pixel geolocation, monthly images of gridded ascending minus descending Tb maps were checked using the final roll, pitch, yaw, delta EIA and timing offset values for each sensor and compared to maps based on the original TDR data. The results showed consistent improvement over the original data

2) Implementation of multiple intercalibration approaches. The use of multiple approaches was done in part to check for consistency between independent calibration techniques. The resulting differences are generally within 0.5K for all channels. Differences tend to be larger for warm scenes and for the older sensors (F08 and F10), but are generally quite consistent.

3) Comparison with other SSM/I FCDR datasets. To date there are three SSM/I FCDR datasets including the CSU dataset, one produced by Remote Sensing Systems, and one produced by Eumetsat's climate monitoring satellite applications facility (CM-SAF). Comparisons of pixel geolocation and EIA with the CM-SAF show generally good agreement, while there are differences with the RSS results. All three FCDR datasets use different standards for the calibration, with the CSU intercalibrating to GPM GMI and the CM-SAF to F11. RSS appears to use a minimization based on their radiative transfer model and in-situ observations, although this is not completely clear.

4) Application to geophysical retrievals. We are working with several different thematic CDR or TCDR developers to use the CSU FCDR with their algorithms. That effort is ongoing, but since the ultimate measure the FCDR is the consistency of the TCDRs or geophysical retrievals, we will continue to work to solicit feedback from various communities. We have also run two different in house retrieval algorithms to test the consistency of the SSM/I FCDR. Figure 6 shows time series of TPW, ocean wind speed, and cloud liquid water over oceans from the complete SSM/I data record. This retrieval over non-precipitating ocean scenes is based on an optimal estimation approach developed by Elsaesser and Kummerow (2008). While the current implementation of this algorithm is not independently validated as a TCDR, it is physical retrieval that accounts for changes in EIA between sensors and is very sensitive to calibration differences, making it a useful tool for analyzing the consistency of the FCDR data record. Finally, the latest operational GPROF precipitation retrieval algorithm (Kummerow et al. 2001, 2011) has been applied to the SSM/I FCDR. While these results are not shown here, they are available from (http://rain.atmos.colostate.edu/RAINMAP). Both the non-raining and raining time series show some differences, but it is important to remember that the six DMSP spacecraft with SSM/I sensors have different local observing times that drift/decay over time leading to diurnal cycle differences. A comparison of GPROF rainfall estimates based on coincident overpasses with TRMM TMI indicates mean rainfall differences between the SSM/I sensors and with TMI of less than 1%, which is below the mean sampling variability of this metric.

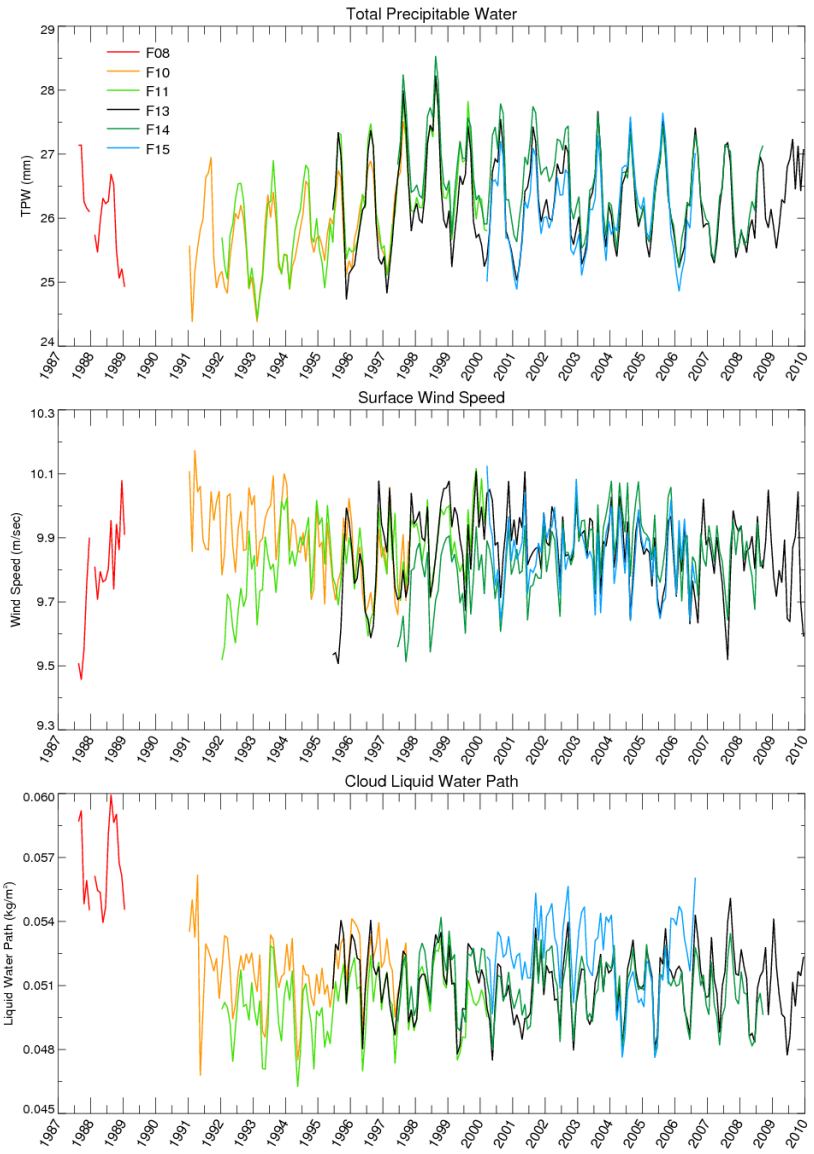


Figure 6: Time series of a) total precipitable water, b) ocean surface wind speed, and c) cloud liquid water path based on the SSM/I FCDR.

## 5.6 Processing Environment and Resources

The code was run in a processing environment described in Table 3.

| | |
|---|---|
| **Hardware** | Dell PowerEdge Server |
| **Memory** | 64GB |
| **Operating system** | CentOS Linux release 8 (64-bit) |
| **Programming language** | C |
| **Hardware** | Dell PowerEdge Server |

| | |
|---|---|
| **Memory** | 64 GB |
| **Processor** | 18 dual core Intel Xeon CPU E5-2695 @ 2.1 GHz (Hyperthreading enabled so appears as 72 CPUs) |
| **Operating system** | CentOS Linux release 8 (64-bit) |
| **Programming language** | C |
| **Compiler** | icc (64-bit) |
| **External libraries** | hdf5, netcdf, mfhdf, df, hdf5_hl, jpeg, z, imf |

**Table 3:** Processing Environment

The code has been designed to facilitate running it on different platforms by means of the following methods:

1. The Makefile, which controls the build process, including compiling and linking.

2. The code is platform-independent. It was compiled and run using the Intel icc compiler, however, it has also been tested and run using the free gnu gcc compiler.

3. The platform-dependent parts of the code are separated from the rest and found in the file `sgdp4h.h`. This file contains code to:

    a. Detect the platform;
    b. For functions that will be used from platform-dependent built-in libraries, load the relevant libraries;
    c. Handle the precision differences of data types on different platforms.

To build the code in a new environment, follow these steps:

1. Ensure that the required external libraries listed in Table 3 are installed (for hdf, netcdf, jpeg, z, imf).

2. Examine the Makefile and set the compiler command if different for the new environment. Also comment/uncomment lines if necessary to select 32-bit or 64-bit environments.

3. Run the make command to create the executable program `ssmi_fcdr` from the source code.

Performance:

1. Using a single CPU on the system detailed above takes approximately 3 seconds wall clock time to run a single file.

2. The entire SSM/I FCDR data record can be reprocessed within a few days.

3. No temporary storage is required to run the algorithm. The only storage required is for the input and output files. The software with the necessary correction files etc. is less than 200 Mbytes.

# 6. Assumptions and Limitations

## 6.1 Algorithm Performance

With the SSM/I sensors, only F15 is still operating and that is in a degraded mode due to the activation of the RADCAL beacons in August 2006 as described in section 3.2.8 and in Milburger and Berg (2012). Note that the performance of the F15 Tb continues to degrade over time. As described in this document the resulting RADCAL corrected data is unsuitable for climate applications and should be used with caution.

## 6.2 Sensor Performance

The sensitivity of the SSM/I instruments is shown in Table 1 and is 0.6 K for the low-resolution channels and 1.1 K for the high-resolution channels. A detailed evaluation of the SSM/I instrument on F08 by Hollinger et al. (1990) also considers gain stability, calibration target stability, spin rate stability, antenna beam characteristics, absolute calibration, and geolocation error and concludes that the F08 SSM/I's sensitivities and

stabilities meet or exceed prelaunch performance specifications, except for the degradation and eventual failure of the 85V channel. Colton and Poe (1999) provides an analysis of sensor performance for all SSM/I sensors, which gives similar results as seen for F08.

# 7. V2 Enhancements

Several enhancements were implemented for the V2 FCDR processing.

### 7.1.1 Intercalibration reference sensor

The original V1 FCDR dataset included a relative intercalibration correction using DMSP F13 as the reference. This was done since there was no community consensus regarding an absolute calibration reference for microwave sensors. Since then, the launch and Cal/Val of the GPM GMI instrument have shown it to be extremely well calibrated and stable for all channels.

### 7.1.2 Cross-track bias corrections

The cross-track bias corrections were updated to include the impact of physical Tb variations across the scan due to roll and pitch variations in the spacecraft attitude. The correction to the edge-of-scan falloff was updated based on both cold and warm scene analysis to provide consistent Tb across the scan regardless of scene temperature.\

### 7.1.3 Geolocation

Updated geolocation and EIA values based on improved roll and pitch sensor mount offsets from scan bias patterns along with updated pitch, yaw, delta EIA and timing offsets.

### 7.1.4 Warm scene intercalibration

Both cold and warm-scene intercalibration corrections were developed/applied for the SSMI window channels.

# 8. Future Enhancements

Quality control is always an issue that could be improved, particularly for the early SSM/I instruments (i.e. F08 and F10) the primary goal for future enhancements should be to address issues identified by users.

# 9. References

Berg, W., R. Kroodsma, C. D. Kummerow and D. S. McKague, 2018: Fundamental Climate Data Records of Microwave Brightness Temperatures, *Remote Sensing*, 10, 1306, doi: 10.3390/rs10081306.

Berg, W. et al., 2016: Intercalibration of the GPM Microwave Radiometer Constellation, *J. Atmos. Oceanic Technol.,* 33, 2639-2654, doi: 10.1175/JTECH-D-16-0100.1.

Berg, W., C. Kummerow, M. Sapiano, N. Rodriguez-Alvarez, and F. Weng, A Fundamental Climate Data Record of Microwave Brightness Temperature data from 25 Years of SSM/I and SSMIS Observations, *GEWEX Newsletter*, August 2012.

Berg, W. K. and N. Rodriguez-Alvarez, 2013: SSM/I Quality Control, Technical Report, Colorado State University, http://rain.atmos.colostate.edu/FCDR/.

Berg, W., M. R. P. Sapiano, J. Horsman, and C. Kummerow, 2013: Improved geolocation and Earth incidence angle information for a fundamental climate data record of the SSM/I sensors, *IEEE Trans. Geosci. Rem. Sens.,* 51, 1504-1513.

Clough, S. A. et al, 2005: Atmospheric Radiative Transfer Modeling: A Summary of the AER Codes, J. Quantitative Spectroscopy and Radiative Transfer, 91, 233-244, doi: 10.1016/j.jqsrt.2004.05.058.

Colton, M. C. and Poe, G. A., 1999: Intersensor calibration of DMSP SSM/I's: F-8 to F-14, 1987-1997*, IEEE Trans. Geosci. Rem. Sens.,* 37(1), 418–439.

Deblonde, G., and S. J. English, 2001: Evaluation of the FASTEM-2 fast microwave ocean surface emissivity model. Tech. Proc. Int. TOVS Study Conf. XI, Budapest, Hungary, WMO, 67–78.

Elsaesser, G. S and C. D. Kummerow, 2008: Toward a fully parametric retrieval of the nonraining parameters over the global oceans, *J. Appl. Meteor. Climatol*., 47, 1599-1618.

Hilburn, K., 2009: Including temperature effects in the F15 RADCAL correction, Technical Report 051209, Remote Sensing Systems, http://www.remss.com.

Hilburn, K. A. and Wentz, F. J., 2008: Mitigating the impact of RADCAL beacon contamination on F15 SSM/I ocean retrievals, *Geophys. Res. Let.,* 35.

Hollinger, J., Lo, R., and Poe, G., 1987: Special Sensor Microwave/Imager User's Guide, Naval Research Laboratory, Washington, D.C.

Hollinger, J. P., Peirce, J. L., and Poe, G. A., 1990: SSM/I Instrument Evaluation, *IEEE Transactions on Geoscience and Remote Sensing*, 28(5), 781–790.

Hollinger, J., 1989: DMSP Special Sensor Microwave/Imager Calibration/Validation, Naval Research Laboratory, Washington, D.C., Vol 1.

Hollinger, J., 1991: DMSP Special Sensor Microwave/Imager Calibration/Validation, Naval Research Laboratory, Washington, D.C., Vol 2.

Kohn, D. J., 1995: Refinement of a semi-empirical model for the microwave emissivity of the sea surface as a function of wind speed. M.S. thesis, Dept. of Meteorology, Texas A&M University, 44 pp.

Kroodsma, R., W. Berg and T. Wilheit, 2021: Updated calibration corrections for V07 of the intercalibrated SSMIS Level 1C data, in prep.

Kummerow, C. D., S. Ringerud, S. Crook, D. Randel, and W. Berg, 2011: An observationally generated a-priori database for microwave rainfall retrievals, *J. Atmos. Oceanic Technol.,* 28, 113-130.

Kummerow, C. D. and Coauthors, 2001: The Evolution of the Goddard Profiling Algorithm (GPROF) for rainfall estimation from passive microwave sensors. *J. Appl. Meteor*., 40, 1801–1820.

Milberger, K. and W. Berg, 2012: SSM/I F15 RADCAL Correction for Ocean Data. Technical Report, Colorado State University, http://rain.atmos.colostate.edu/FCDR/.

Meisner, T. and F. J. Wentz, 2012: The Emissivity of the Ocean Surface Between 6 and 90 GHz Over a Large Range of Wind Speeds and Earth Incidence Angles, *IEEE Trans. Geosci. Rem. Sens.*, 50, 3004-3026, doi: 10.1109/TGRS.2011.2179622.

Poe, G. A., Uliana, E., Gardiner, B. and vonRentzell, T., 2006: Mitigation of DMSP F-15 RADCAL Interference with SSM/I, Technical report, NRL, Monterey, CA. Code 7541.

Raytheon Company. Special Sensor Microwave/Imager (SSM/I) User's Interpretation Guide, UG32268-900, Revision C, 29 Nov 2000.

Rosenkranz, P. W., 1998: Water vapor microwave continuum absorption: A comparison of measurements and models. *Radio Sci.,* 33, 919–928.

Sapiano, M. R. P., 2012: Intercalibration of SSM/I and SSMIS for the CSU FCDR. Technical Report, Colorado State University, http://rain.atmos.colostate.edu/FCDR/.

Sapiano, M. R. P. and Berg, W., 2012: Estimation of Satellite Attitude for SSM/I and SSMIS Geolocation. Technical Report, Colorado State University, http://rain.atmos.colostate.edu/FCDR/.

Sapiano, M. R. P., Berg, W. K., McKague, D. S., and Kummerow, C. D., 2013: Towards an Intercalibrated Fundamental Climate Data Record of the SSM/I Sensors, *IEEE Trans. Geosci. Remote Sens.*, 51, 1492-1503.

Sapiano, M. R. P., Bilanow, S., and Berg, W. K., 2011: SSM/I and SSMIS Stewardship Code Geolocation Algorithm Theoretical Basis. Technical Report, Colorado State University, http://rain.atmos.colostate.edu/FCDR/.

Stogryn, A. P., Butler, C. T. and Bartolac, T. J., 1994: Ocean surface wind retrievals from special sensor microwave imager data with neural networks, *J. Geophys. Res*., 99(C1), 981–984.

Vallado, D. A., Crawford, P., Hujsak, R., and Kelso, T. S., Revisiting Spacetrack Report #3, presented at the AIAA/AAS Astrodynamics Specialist Conference, Keystone, CO, 2006 August 21–24.

Wentz, F. and D. Draper, 2016: On-orbit Absolute Calibration of the Global Precipitation Mission Microwave Imager, *J. Atmos. Ocean. Technol.,* 33, 1393-1412, doi: 10.1175/JTECH-D-15-0212.1.

Wilheit, T. T., 1979a: A model for the microwave emissivity of the ocean's surface as a function of wind speed. *IEEE Trans. Geosci. Electron.,* 17, 244**–**249.

Wilheit, T. T., 1979b: The effect of wind on the microwave emission from the ocean's surface at 37 GHz., *J. Geophys. Res*., 84, 4921-4926.

# Appendix A. Acronyms and Abbreviations

| Acronym or Abbreviation | Definition |
|---|---|
| ANSI | American National Standards Institute |
| APC | Antenna Pattern Correction |
| C-ATBD | Climate Algorithm Theoretical Basis Document |
| CDR | Climate Data Record |
| DMSP | Defense Meteorological Satellite Program |
| FCDR | Fundamental Climate Data Record |
| FOC | Full Operating Capability |
| FNMOC | Fleet Numerical Meteorology and Oceanography Center |
| GPSr9 | SSMIS Ground Processing Software revision 9 |
| ICD | Interface Control Document |
| IEEE | Institute of Electrical and Electronic Engineers |
| IOC | Initial Operating Capability |
| LAS | Lower Atmospheric Sounding |
| NCDC | National Climatic Data Center |
| NOAA | National Oceanic and Atmospheric Administration |
| NRL | Naval Research Laboratory |
| OAD | Operational Algorithm Description |
| SDR | Sensor Data Record (contains Tb data) |
| SGP4 | Simplified General Perturbations orbital model |
| SSM/I | Special Sensor Microwave/Imager |
| SSMIS | Special Sensor Microwave Imager/Sounder |
| TA | Antenna Temperature |
| TB | Brightness Temperature |
| TDR | Temperature Data Record (contains Ta data) |
| TLE | Two Line Element |
| UAS | Upper Atmospheric Sounding |